XXXVI Ibero-Latin American Congress on Computational Methods in Engineering
CILAMCE
Rio de Janeiro, 22-25 Nov 2015

SOLUTION OF THE LWR NONLINEAR TRAFFIC FLOW MODEL USING A DISCONTINUOUS GALERKIN FEM APPROACH

Alberto Costa Nogueira Junior

Jonathan Bernardo

albercn@br.ibm.com

jobern@br.ibm.com

IBM Research Brazil

Rua Tutóia, 1157, 04007-900, São Paulo, SP, Brazil

Stephen Moore

stevemoore@au1.ibm.com

IBM Research Australia

380 La Trobe st., 13th floor, Melbourne VIC 3000, Australia

Abstract. *In this article, we propose a high-order discontinuous Galerkin finite element (DG-FEM) discretization to solve the classical LWR traffic flow model. The monotone Lax-Friedrichs flux was chosen to compute numerical fluxes. Numerical stability was added to the scheme through over integration of the nonlinear physical flux. A sub-cell shock capturing mechanism with localized artificial viscosity was also used to stabilize solutions in the presence of shock discontinuities. To deal with the* 2^{nd} *order differential operator associated to the artificial dissipation, the LDG (Local Discontinuous Galerkin) method was employed. Numerical examples were computed for smooth and discontinuous initial conditions. The DG-FEM scheme was compared to the following standard discretizations: the* 2^{nd} *order MacCormack finite difference (FD) scheme, the standard* 1^{st} *order finite volume (FV) method and the* 2^{nd} *order MUSCL scheme. The sub-cell shock capturing mechanism, commonly used in aerospace applications, proved to be very sharp and reliable to stabilize solutions which develop shock discontinuities although it can over smear the shock profile when the approximate solution evolves for long time periods. Overall, DG-FEM approach revealed to be more accurate, robust and flexible to solve the LWR traffic equation when compared to their above mentioned competitors.*

Keywords: *High-order, discontinuous Galerkin, finite element, shock capturing, traffic flow.*

1 INTRODUCTION

Traffic flow can be modeled by a typical conservation law like the fluid dynamics continuity equation. One of the most popular traffic flow models is the LWR scheme due to Lighthill, Witham and Richards (Lighthill et al., 1955, Richards, 1956). This is a fairly accurate model even if it holds only for long crowded roads with a large number of vehicles (Ceulemans et al., 2009).

In this article, we propose a high-order discontinuous Galerkin finite element (DG-FEM) discretization to solve the classical LWR traffic flow model. The monotone Lax-Friedrichs flux was chosen to compute numerical fluxes. As usual in the DG-FEM formulation, Dirichlet or Neumann boundary conditions were weakly imposed at the boundaries of the domain. Numerical stability was added to the scheme through over integration of the nonlinear physical flux, and a sub-cell shock capturing mechanism with localized artificial viscosity was used to stabilize solutions in the presence of discontinuities. To discretize the 2^{nd} order differential operator associated to the artificial dissipation, the Local Discontinuous Galerkin (LDG) method was employed. A different approach for the solution of the traffic flow model on networks using limiters to stabilize the DG-FEM formulation in the presence of shock discontinuities can be found in (Suncica et al., 2015).

The present DG-FEM implementation allows for two different polynomial basis, the Lagrange nodal basis (Hesthaven et al., 2008) and the Legendre modal basis (Karniadakis et al., 2005). Each basis shows strengths and weaknesses for the numerical approximation of the problem solution but the modal basis received special attention due to its orthogonality property which makes the shock sensor implementation straightforward.

Numerical examples were computed for smooth and discontinuous initial conditions. The proposed DG-FEM scheme was compared to two different discretization schemes, namely, Finite Difference Method (FDM) (LeVeque, 2007) and Finite Volume Method (FVM) (LeVeque, 1990; Hirsch, 1990). In the former case, the 2^{nd} order MacCormack scheme (MacCormack, 1969) was implemented and, for the latter, the standard 1^{st} order scheme and the 2^{nd} order MUSCL (Van Leer, 1979) scheme were used. Compared to the other discretizations, DG-FEM demonstrated to be a good choice due to its high order approximation properties like exponential convergence and computational benefits like compact support. For many numerical schemes, high order approximation is a well suited feature since it produces more accurate results and, potentially, better physical representations.

The sub-cell shock capturing mechanism (Persson et al., 2006, Barter et al., 2010, Klöckner et al., 2011), typically used in aerospace applications, proved to be very sharp and reliable to stabilize solutions which develop shock discontinuities although it can over smear the shock profile when the approximate solution evolves for long time periods. When dealing with smooth solutions the DG-FEM scheme revealed much superior than the its competitors due to its ability to represent these mathematical behavior through high order polynomial approximations. Overall, the DG-FEM approach revealed to be quite accurate, robust and flexible to solve the LWR traffic equation.

2 THE LWR TRAFFIC FLOW MODEL

Traffic flow models seek to describe the everyday experiences of the roads with mathematics, to help engineers design better road systems. In this article we consider the Lighthill-Whitham-

Richards (LWR) traffic flow model described by the following hyperbolic conservation law,

$$\frac{\partial u(x,t)}{\partial t} + \frac{\partial f(u(x,t))}{\partial x} = 0, \; x \in [L,R] = \Omega, \tag{1}$$

with appropriate initial and boundary conditions given by

$$u(x,0) = u_0(x), \; u(L,t) = u_L(t), \; u(R,t) = u_R(t), \tag{2}$$

where $u(x,t)$ is the traffic density, $x \in \mathbb{R}$ and $t \in \mathbb{R}_+$ are the space and time coordinates and Ω is the problem domain, respectively.

The LWR model considers cars with a continuous traffic density (average number of cars per unit length of road) rather than keeping track of them individually. A basic assumption of this model is that the car speed is a monotonically decreasing function of car density resulting in a nonlinear quadratic traffic flux, $f(u)$ (Fig. 1).

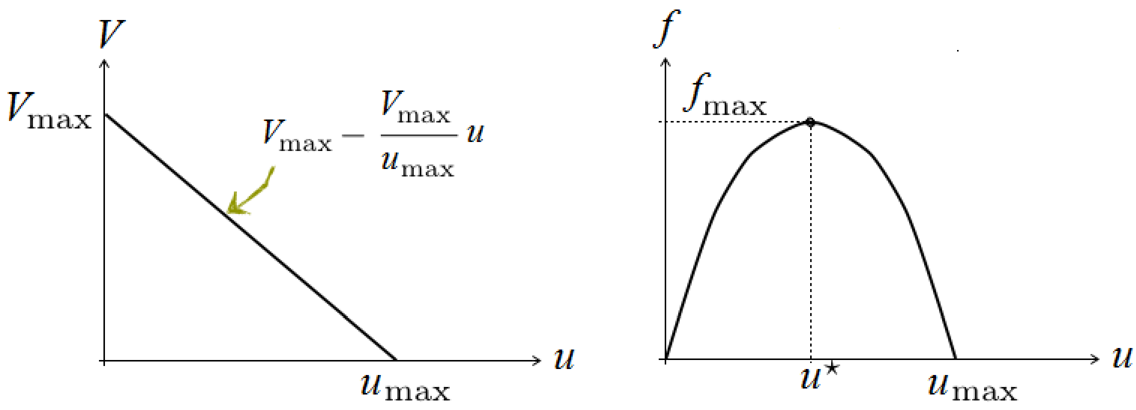

Figure 1: Monotonically decreasing car speed and quadratic traffic flux

The typical quadratic flux function $f : \mathbb{R} \to \mathbb{R}$ used in this model is that due to Greenshiels (Greenshiels, 1935) which can be written as

$$f(u) = uV_{max}\left(1 - \frac{u}{u_{max}}\right) \tag{3}$$

where the constants V_{max} and u_{max} stand for maximum car speed and maximum car density, respectively.

3 THE DG-FEM APPROACH

3.1 The weak formulation

In order to obtain an approximation for the solution of the Eq. (1), we will rewrite the previous initial-boundary value problem in an integral form. For this, we assume that our integral form will be valid for each individual element of a given mesh and the global approximate solution will be enforced by a numerical flux that allows inter element communication through their boundaries. Using this premise, for each element Ω^k of the mesh, we form the local residual as follows

$$x \in \Omega^k : \mathcal{R}_h(x,t) = \frac{\partial u_h^k}{\partial t} + \frac{\partial f_h^k}{\partial x}, \tag{4}$$

where u_h^k and f_h^k are numerical approximations to the conserved quantity, $u(x,t)$, and the physical flux, $f(u)$, respectively. As in every Galerkin finite element formulation, we require that the residual is orthogonal to all test functions $\phi_j^k(x)$ belonging to a vector space $V_h^k \subset P(\Omega^k)$, where $P(\Omega^k)$ is a suitable finite-dimensional approximation space on the element Ω^k, such as the polynomials $\mathcal{P}_p$ of up to degree p:

$$\int_{\Omega^k} \mathcal{R}_h(x,t)\phi_j^k(x)\,dx = 0, \tag{5}$$

Substituting the residual expression into the orthogonal relation yields

$$\int_{\Omega^k} \frac{\partial u_h^k}{\partial t}\phi_j^k(x) + \frac{\partial f_h^k}{\partial x}\phi_j^k(x)\,dx = 0. \tag{6}$$

Integrating the second term of (6) by parts once gives us the weak local statement of the traffic flow problem

$$\int_{\Omega^k} \left(\frac{\partial u_h^k}{\partial t}\phi_j^k(x) - f_h^k \frac{d\phi_j^k}{dx} \right) dx = -\left[f_h^k \phi_j^k \right]_{x_l^k}^{x_r^k}. \tag{7}$$

3.2 Discretization of the weak formulation

We approximate Ω by K nonoverlapping elements, $x \in [x_l^k, x_r^k] = \Omega^k$. On each of these elements we will assume that the local traffic density solution, $u_h^k(x,t)$, and the local flux, $f_h^k(u_h(x,t))$, can be expressed as a polynomial of order N

$$x \in \Omega^k : \; u_h^k(x,t) = \sum_{j=1}^{N+1} \hat{u}_j^k(t)\psi_j^k(x), \tag{8}$$

$$f_h^k(u_h(x,t)) = \sum_{j=1}^{N+1} \hat{f}_j^k(t)\psi_j^k(x). \tag{9}$$

where $\psi_j^k(x)$ are the local basis functions which can be chosen as of the modal or nodal type. In this work we consider the Legendre polynomials, $P_n(\xi)$, defined on the reference interval $[-1,1]$, for the modal basis and the Lagrange polynomials, $\ell_i^k(x)$, defined through the $N_p = N+1$ Gauss-Legendre-Lobatto quadrature points, for the nodal case. These two basis functions representations are connected by the definition of the expansion coefficients, $\hat{u}_i$, as follows

$$\mathcal{V}\hat{\boldsymbol{u}} = \boldsymbol{u} \tag{10}$$

where $\mathcal{V}_{ij} = P_{j-1}(\xi_i)$, $\hat{\boldsymbol{u}}_i = \hat{u}_i$, $\boldsymbol{u}_i = u(\xi_i)$. The matrix $\mathcal{V}$ is recognized as the generalized Vandermond matrix.

Now we return to the Eq. (7) and replace the arbitrary test function ϕ_j^k by the piecewise polynomial functions $\psi_i^k(x) \in V_h^k$. We also introduce the numerical flux f^* in order to recover the global meaning of the DG-FEM approximate solution of the traffic flow problem. Now, the semi-discrete form of the DG-FEM formulation can be written as

$$\int_{\Omega^k} \left(\frac{\partial u_h^k}{\partial t} \psi_i^k(x) - f_h^k(u_h^k) \frac{d\psi_i^k(x)}{dx} \right) dx = - \left[\psi_i^k(x) f^* \right]_{x_l^k}^{x_r^k}, \ 1 \leq i \leq N+1. \tag{11}$$

Substituting the right hand side of expressions (8) and (9) into the last equation and using an affine transformation to perform integrations on the reference element $\hat{\Omega} = [-1, 1]$, we can rewrite the semi-discrete DG-FEM weak formulation in its matrix form,

$$\mathcal{M}^k \frac{d}{dt} \hat{\boldsymbol{u}}_h^k - \mathcal{S}^T \hat{\boldsymbol{f}}_h^k = -\hat{\boldsymbol{\psi}}(\xi_r) f^*(x_r^k, x_l^{k+1}) + \hat{\boldsymbol{\psi}}(\xi_l) f^*(x_l^k, x_r^{k-1}), \tag{12}$$

where, for $1 \leq i, j \leq N+1$,

$$\mathcal{M}_{ij}^k = \frac{h^k}{2} \int_{\hat{\Omega}} \hat{\psi}_i \hat{\psi}_j \, d\xi, \tag{13}$$

$$\mathcal{S}_{ij} = \int_{\hat{\Omega}} \hat{\psi}_i \frac{d\hat{\psi}_j}{d\xi} \, d\xi, \tag{14}$$

are the local mass and stiffness matrices, respectively. The term $h^k/2$ is the jacobian associated to the affine transformation and its value is half of the size of the k-th element, Ω^k. Furthermore, we have

$$\hat{\boldsymbol{u}}_h^k = [\hat{u}_1^k, \ldots, \hat{u}_{N+1}^k]^T, \tag{15}$$

$$\hat{\boldsymbol{f}}_h^k = [\hat{f}_1^k, \ldots, \hat{f}_{N+1}^k]^T, \tag{16}$$

$$\hat{\boldsymbol{\psi}} = [\hat{\psi}_1(\xi), \ldots, \hat{\psi}_{N+1}(\xi)]^T. \tag{17}$$

as the vectors of local traffic density coefficients, flux coefficients and local test functions, respectively.

3.3 Local recovering of the nonlinear flux coefficients

We have chosen to represent the physical flux $f(u)$ as a polynomial expansion of the local basis functions $\psi_j^k(x)$ analogously to what we have done for the conserved quantity u. This definition implies increasing the total number of degrees of freedom of the approximate solution. In order to alleviate this inconvenient, we rewrite f_h^k in terms of the approximate solution u_h^k and apply a L^2 projection to locally recover $\hat{f}_i^k$ coefficients. We propose a three step algorithm to accomplish this task:

1. Evaluate the approximate solution, $u_h^k(x,t)$, at $Q_n = ceil(\frac{3N+1}{2})$ quadrature points

$$u_h^k(x_l, t) = \sum_{i=1}^{N+1} \hat{u}_i(t) \hat{\psi}_i(\xi_l), \ 1 \leq l \leq Q_n.$$

2. Evaluate the quadratic flux, f_h^k, using u_h^k computed in the previous step

$$f_h^k(x_l,t) = V_{max}\left(u_h^k(x_l,t) - \frac{(u_h^k(x_l,t)^2)}{u_{max}}\right),\ 1 \leq l \leq Q_n.$$

3. Project the nonlinear flux into the polynomial space

$$f_h^k(x,t) = \sum_{j=1}^{N+1} \hat{f}_j^k(t)\psi_j(x)$$
$$\sum_{j=1}^{N+1} \hat{f}_j^k(t)\int_{\Omega^k}\psi_i(x)\psi_j(x)\,dx = \int_{\Omega^k} f_h^k(x,t)\psi_i(x)\,dx,\ 1 \leq i \leq N+1$$
$$\sum_{j=1}^{N+1} \hat{f}_j^k(t)\frac{h^k}{2}\int_{\hat{\Omega}}\hat{\psi}_i(\xi)\hat{\psi}_j(\xi)\,d\xi = \frac{h^k}{2}\int_{\hat{\Omega}} f_h^k(x(\xi),t)\hat{\psi}_i(\xi)\,d\xi,\ 1 \leq i \leq N+1$$
$$\mathcal{M}\hat{\boldsymbol{f}}^k = \boldsymbol{b}^k \Rightarrow \hat{\boldsymbol{f}}^k = \mathcal{M}^{-1}\boldsymbol{b}^k.$$

where

$$\mathcal{M}_{ij} = \int_{\hat{\Omega}} \hat{\psi}_i\hat{\psi}_j\,d\xi, \tag{18}$$
$$\boldsymbol{b}_i^k = \int_{\hat{\Omega}} f_h^k(x(\xi),t)\hat{\psi}_i(\xi)\,d\xi, \tag{19}$$

are the local mass matrix and the local load vector defined on the reference element $\hat{\Omega}$, respectively.

We evaluate Eq. (19) at Q_n quadrature points in order to consistently integrate the vector $\boldsymbol{b}^k$ since the nonlinear flux and the basis functions are at most polynomials of degree $2N$ and N, respectively. Equation (18) can be evaluated at $Q_l = ceil(\frac{2N+1}{2})$ quadrature points as the basis functions multiplied by each other result in a polynomial of degree $2N$ at most. This strategy adds stability to the whole numerical scheme.

3.4 Numerical flux definition

We consider the monotone Lax-Friedrichs flux in order to stabilize the present DG-FEM discretization

$$f^*(u_h^-, u_h^+) = \{\{f_h(u_h)\}\} + \frac{C}{2}[[u_h]], \tag{20}$$

where $C = \max|f_u|$ is an upper bound on the local traffic wave speed and $\{\{.\}\}$ and $[[.]]$ are the average and jump operators usually defined as follows

$$\{\{u\}\} = \frac{u^- + u^+}{2} \tag{21}$$

where u can be both a scalar or a vector quantity and

$$[[u]] = \hat{\mathbf{n}}^- u^- + \hat{\mathbf{n}}^+ u^+, \tag{22}$$
$$[[\mathbf{u}]] = \hat{\mathbf{n}}^- \cdot \mathbf{u}^- + \hat{\mathbf{n}}^+ \cdot \mathbf{u}^+ \tag{23}$$

where $\hat{\mathbf{n}}$ is the normal vector along the left or right boundaries of the k element. We observe that the jump operator is defined differently depending on whether u is a scalar or a vector, $\mathbf{u}$. The superscripts "$-$" and "$+$" stand for the interior and exterior information of the element, respectively.

The upper bound C can easily be estimated as

$$C = \max|\frac{\partial f}{\partial u}| = \max\left|V_{max}\left(1 - \frac{2u}{u_{max}}\right)\right|. \tag{24}$$

We finally substitute the definition (20) into the right hand side of the Eq. (12) to get the final semi-discrete form of the traffic flow problem

$$\begin{aligned}\frac{h^k}{2}\mathcal{M}\frac{d}{dt}\hat{\boldsymbol{u}}_h^k - \mathcal{S}^T\hat{\boldsymbol{f}}_h^k = & \left[-\frac{1}{2}\mathcal{F}_l^{k+1}\left(\hat{\boldsymbol{f}}_h^{k+1} - C\hat{\boldsymbol{u}}_h^{k+1}\right) - \frac{1}{2}\mathcal{F}_r^k\left(\hat{\boldsymbol{f}}_h^k + C\hat{\boldsymbol{u}}_h^k\right)\right. \\ & \left. + \frac{1}{2}\mathcal{F}_r^{k-1}\left(\hat{\boldsymbol{f}}_h^{k-1} + C\hat{\boldsymbol{u}}_h^{k-1}\right) + \frac{1}{2}\mathcal{F}_l^k\left(\hat{\boldsymbol{f}}_h^k - C\hat{\boldsymbol{u}}_h^k\right)\right].\end{aligned} \tag{25}$$

where

$$\begin{aligned}\mathcal{F}_r^k &= [\hat{\boldsymbol{\psi}}(1) \otimes \hat{\boldsymbol{\psi}}(1)], \\ \mathcal{F}_l^{k+1} &= [\hat{\boldsymbol{\psi}}(1) \otimes \hat{\boldsymbol{\psi}}(-1)], \\ \mathcal{F}_l^k &= [\hat{\boldsymbol{\psi}}(-1) \otimes \hat{\boldsymbol{\psi}}(-1)], \\ \mathcal{F}_r^{k-1} &= [\hat{\boldsymbol{\psi}}(-1) \otimes \hat{\boldsymbol{\psi}}(1)].\end{aligned}$$

are the *Lift* matrices associated to the boundaries of each element. These matrices are defined as the dyadic product of two vectors of elemental basis functions evaluated at the boundaries of the standard element $\hat{\Omega}$.

3.5 Viscous formulation of the LWR model

To control numerical wiggles around shocks we adopt a strategy commonly used in aerodynamic applications which introduces small quantities of artificial viscosity into the problem solution. In the context of traffic flow problems, this technique requires the addition of a second order diffusive term at the right hand side of the original Eq. (1) as follows

$$\frac{\partial u}{\partial t} + \frac{\partial f(u)}{\partial x} = \frac{\partial}{\partial x}\varepsilon(x)\frac{\partial u}{\partial x}, \tag{26}$$

where $\varepsilon(x)$ is the artificial viscosity function. This equation must be subjected to appropriate initial and boundary conditions.

In order to develop a suitable DG discretization for this second order PDE, we rewrite the last statement as a system of first order equations

$$\begin{aligned}&\frac{\partial u}{\partial t} + \frac{\partial}{\partial x}(f(u) - \sqrt{\varepsilon}q) = 0 \\ &q = \sqrt{\varepsilon}\frac{\partial u}{\partial x}\,.\end{aligned} \tag{27}$$

As before, we write approximations for the variables u, f and q, and multiply both equations by arbitrary test functions ϕ_j^k and integrate them over each element Ω^k to get the local weak statement of the modified traffic flow problem

$$\int_{\Omega^k} \frac{\partial u_h^k}{\partial t}\phi_j^k\, dx - \int_{\Omega^k} f_h^k \frac{\partial \phi_j^k}{\partial x}\, dx + \int_{\Omega^k} (\sqrt{\varepsilon} q_h^k)\frac{\partial \phi_j^k}{\partial x}\, dx = -\left[f_h^k \phi_j^k\right]_{x_l^k}^{x_r^k} + \left[(\sqrt{\varepsilon} q_h^k)\phi_j^k\right]_{x_l^k}^{x_r^k}, \tag{28}$$

$$\int_{\Omega^k} q_h^k \phi_j^k\, dx + \int_{\Omega^k} u_h^k \frac{\partial}{\partial x}(\sqrt{\varepsilon}\phi_j^k)\, dx = \left[(\sqrt{\varepsilon} u_h^k)\phi_j^k\right]_{x_l^k}^{x_r^k}\ . \tag{29}$$

In order to discretize the later system of equations using the DG approach we assume

$$q_h^k(x,t) = \sum_{j=1}^{N+1} \hat{q}_j^k(t)\psi_j^k(x), \tag{30}$$

in exactly the same way we did for $u_h^k(x,t)$ and $f_h^k(u_h(x,t))$ in Eqs. (8) and (9).

Substituting Eqs. (8), (9) and (30) in the system above, replacing the arbitrary test function ϕ_j^k by the piecewise polynomial functions $\psi_i^k(x)$ and introducing the numerical fluxes f^*, $(\sqrt{\varepsilon}q)^*$ and $(\sqrt{\varepsilon}u)^*$ at the element interfaces, we get the DG-FEM semi-discrete form of the modified traffic flow problem

$$\sum_{j=1}^{N+1} \int_{\Omega^k} \frac{d\hat{u}_j^k}{dt}\psi_j^k\psi_i^k\, dx - \sum_{j=1}^{N+1}\int_{\Omega^k} \hat{f}_j^k \psi_j^k \frac{d\psi_i^k}{dx}\, dx + \sum_{j=1}^{N+1}\int_{\Omega^k} \sqrt{\varepsilon}\, \hat{q}_j^k \psi_j^k \frac{d\psi_i^k}{dx}\, dx =$$

$$- \left[\psi_i^k f^*\right]_{x_l^k}^{x_r^k} + \left[\psi_i^k(\sqrt{\varepsilon} q_h^k)^*\right]_{x_l^k}^{x_r^k},\ 1 \le i \le N+1, \tag{31}$$

$$\sum_{j=1}^{N+1} \int_{\Omega^k} \hat{q}_j^k \psi_j^k \psi_i^k\, dx + \sum_{j=1}^{N+1}\int_{\Omega^k} \hat{u}_j^k \psi_j^k \frac{d}{dx}(\sqrt{\varepsilon}\psi_i^k)\, dx = \left[\psi_i^k(\sqrt{\varepsilon} u_h^k)^*\right]_{x_l^k}^{x_r^k},\ 1 \le i \le N+1. \tag{32}$$

To recover the matrix form of the above system, we use the affine mapping to perform integrations on the reference element $\hat{\Omega} = [-1, 1]$ and rewrite the DG-FEM semi-discrete formulation as follows

$$\begin{aligned}\frac{h^k}{2}\mathcal{M}\frac{d}{dt}\hat{\boldsymbol{u}}_h^k - \mathcal{S}^T \hat{\boldsymbol{f}}_h^k + (\mathcal{S}^{\sqrt{\varepsilon}})^T \hat{\boldsymbol{q}}_h^k = &- \hat{\boldsymbol{\psi}}(\xi_r) f^*(x_r^k, x_l^{k+1}) + \hat{\boldsymbol{\psi}}(\xi_l) f^*(x_l^k, x_r^{k-1}) \\ &+ \hat{\boldsymbol{\psi}}(\xi_r)(\sqrt{\varepsilon} q_h^k)^*(x_r^k, x_l^{k+1}) - \hat{\boldsymbol{\psi}}(\xi_l)(\sqrt{\varepsilon} q_h^k)^*(x_l^k, x_r^{k-1}),\end{aligned} \tag{33}$$

$$\frac{h^k}{2}\mathcal{M}\hat{\boldsymbol{q}}_h^k + (\tilde{\mathcal{S}}^{\sqrt{\varepsilon}})^T \hat{\boldsymbol{u}}_h^k = \hat{\boldsymbol{\psi}}(\xi_r)(\sqrt{\varepsilon} u_h^k)^*(x_r^k, x_l^{k+1}) - \hat{\boldsymbol{\psi}}(\xi_l)(\sqrt{\varepsilon} u_h^k)^*(x_l^k, x_r^{k-1}). \tag{34}$$

where $\mathcal{M}$, $\mathcal{S}$ and $\hat{\boldsymbol{\psi}}$ have already been defined by Eqs. (18), (14) and (17), respectively. We observe however that two new operators have been introduced

$$\mathcal{S}_{ij}^{\sqrt{\varepsilon}} = \int_{\Omega^k} \sqrt{\varepsilon}\psi_j^k \frac{d\psi_i^k}{dx}\, dx, \tag{35}$$

$$\tilde{\mathcal{S}}_{ij}^{\sqrt{\varepsilon}} = \int_{\Omega^k} \psi_j^k \frac{d}{dx}(\sqrt{\varepsilon}\psi_i^k)\, dx\ . \tag{36}$$

As before, we use the monotone Lax-Friedrichs flux for the convective numerical flux f^*. For the numerical fluxes $(\sqrt{\varepsilon}q)^*$ and $(\sqrt{\varepsilon}u)^*$, corresponding to the second order dissipative operator, we choose the Local Discontinuous Galerkin (LDG) flux which yields optimal convergence rates. An usual way to define LDG scheme is as follows

$$(\sqrt{\varepsilon}u_h)^* = \{\{\sqrt{\varepsilon}\,\}\}u_h^+,\ (\sqrt{\varepsilon}q_h)^* = \sqrt{\varepsilon^-}q_h^-. \tag{37}$$

The LDG scheme for derivative operators of second order is a smart way to use the upwinding concept for problems that have no preferred direction of propagation (e.g. dissipation and diffusion problems). If fact, the upwinding in this case is done in a very careful way, ensuring that the upwinding for u_h and q_h is always done in opposite directions (Hesthaven et al., 2008).

Now, using the LDG scheme, we can return to the right hand side of Eqs. (33) and (34) and explicitly define the numerical fluxes $(\sqrt{\varepsilon}u_h)^*$ and $(\sqrt{\varepsilon}q_h)^*$ as follows

$$\hat{\boldsymbol{\psi}}(\xi_r)(\sqrt{\varepsilon}u_h^k)^* - \hat{\boldsymbol{\psi}}(\xi_l)(\sqrt{\varepsilon}u_h^k)^* = \hat{\boldsymbol{\psi}}(\xi_r)\{\{\sqrt{\varepsilon}\,\}\}u_h^{k+1}(x_l^{k+1}) - \hat{\boldsymbol{\psi}}(\xi_l)\{\{\sqrt{\varepsilon}\,\}\}u_h^k(x_l^k), \tag{38}$$

$$\hat{\boldsymbol{\psi}}(\xi_r)(\sqrt{\varepsilon}q_h^k)^* - \hat{\boldsymbol{\psi}}(\xi_l)(\sqrt{\varepsilon}q_h^k)^* = \hat{\boldsymbol{\psi}}(\xi_r)\sqrt{\varepsilon(x_r^k)}q_h^k(x_r^k) - \hat{\boldsymbol{\psi}}(\xi_l)\sqrt{\varepsilon(x_r^{k-1})}q_h^{k-1}(x_r^{k-1}). \tag{39}$$

The final matrix form of the semi-discrete DG-FEM approximation of the modified traffic flow problem looks like this:

$$\begin{aligned}\frac{h^k}{2}\mathcal{M}\frac{d}{dt}\hat{\boldsymbol{u}}_h^k - \mathcal{S}^T\hat{\boldsymbol{f}}_h^k + (\mathcal{S}^{\sqrt{\varepsilon}})^T\hat{\boldsymbol{q}}_h^k = &\Big[-\frac{1}{2}\mathcal{F}_l^{k+1}\left(\hat{\boldsymbol{f}}_h^{k+1} - C\hat{\boldsymbol{u}}_h^{k+1}\right) - \frac{1}{2}\mathcal{F}_r^k\left(\hat{\boldsymbol{f}}_h^k + C\hat{\boldsymbol{u}}_h^k\right)\\ &+ \frac{1}{2}\mathcal{F}_r^{k-1}\left(\hat{\boldsymbol{f}}_h^{k-1} + C\hat{\boldsymbol{u}}_h^{k-1}\right) + \frac{1}{2}\mathcal{F}_l^k\left(\hat{\boldsymbol{f}}_h^k - C\hat{\boldsymbol{u}}_h^k\right)\\ &+ \sqrt{\varepsilon(x_r^k)}\,\mathcal{F}_r^k\hat{\boldsymbol{q}}_h^k - \sqrt{\varepsilon(x_r^{k-1})}\,\mathcal{F}_r^{k-1}\hat{\boldsymbol{q}}_h^{k-1}\Big],\end{aligned} \tag{40}$$

$$\begin{aligned}\frac{h^k}{2}\mathcal{M}\hat{\boldsymbol{q}}_h^k + (\tilde{\mathcal{S}}^{\sqrt{\varepsilon}})^T\hat{\boldsymbol{u}}_h^k = &+\frac{1}{2}\left(\sqrt{\varepsilon(x_l^{k+1})} + \sqrt{\varepsilon(x_r^k)}\right)\mathcal{F}_l^{k+1}\hat{\boldsymbol{u}}_h^{k+1}\\ &-\frac{1}{2}\left(\sqrt{\varepsilon(x_r^{k-1})} + \sqrt{\varepsilon(x_l^k)}\right)\mathcal{F}_l^k\hat{\boldsymbol{u}}_h^k.\end{aligned} \tag{41}$$

3.6 Sub-cell shock capturing

The development of the previous alternative formulation of the traffic flow equation with the second order dissipative term is the necessary step to apply the sub-cell shock capturing strategy. The current approach locally introduces dissipation in the vicinity of shocks and the amount of viscosity required for stability is determined by the resolution of the approximating space. A shock detection algorithm based on the rate of decay of the expansion coefficients of the approximated solution is used to track the troubled cells where artificial viscosity is need to ensure stability.

The method used in this work to detect oscillations near shocks was originally proposed by Persson & Peraire (Persson et al., 2006). This method is based on the representation of the high-order approximated solution within each element by hierarchical orthogonal polynomials, namely, Legendre polynomials. The expansion coefficients of the Legendre basis are treated as a sequence of Fourier modes. For smooth solutions the expansion coefficients are expected to decay very rapidly ($\sim 1/N^2$). On the other hand, in the presence of an actual discontinuity all frequency modes are present and the Fourier-like coefficients decrease much more slowly. In this context, solutions of polynomial order N within each element can be represented as

$$u(x) = \sum_{j=1}^{N+1} \hat{u}_j^k \psi_j^k(x),$$

where $\psi_j^k(x)$ are the Legendre polynomials and $\hat{u}_j^k$ are the modal coefficients. For a truncated representation of the same solution at order $N-1$, we write

$$\tilde{u}(x) = \sum_{j=1}^{N} \hat{u}_j^k \psi_j^k(x).$$

With these two representations, the shock indicator is defined as

$$F_k = \frac{\langle u - \tilde{u}, u - \tilde{u} \rangle_k}{\langle u, u \rangle_k}, \tag{42}$$

where $\langle \cdot, \cdot \rangle_k$ represents the standard L^2 inner product over the element k. The indicator can readily be computed if we recover the following expressions

$$\begin{aligned} u - \tilde{u} &= \hat{u}_{N+1}^k \psi_{N+1}^k, \\ \langle u - \tilde{u}, u - \tilde{u} \rangle_k &= \int_{\Omega_k} (\hat{u}_{N+1}^k \psi_{N+1}^k)^2 \, dx, \\ \langle u, u \rangle_k &= \int_{\Omega_k} (\sum_{j=1}^{N+1} \hat{u}_j^k \psi_j^k)^2 \, dx = (\hat{\boldsymbol{u}}_h^k)^T \mathcal{M}^k \hat{\boldsymbol{u}}_h^k. \end{aligned}$$

Once the shock has been detected by the previous indicator, the amount of artificial viscosity is taken to be constant over each element and determined by the following function,

$$\varepsilon_k = \begin{cases} 0 & \text{if } s_k < s_0 - \kappa \\ \frac{\varepsilon_0}{2} \left(1 + \sin \frac{\pi(s_k - s_0)}{2\kappa}\right) & \text{if } s_0 - \kappa \leq s_k \leq s_0 + \kappa \\ \varepsilon_0 & \text{if } s_k > s_0 + \kappa, \end{cases} \tag{43}$$

where $\varepsilon_0 = 0.5 \cdot (max\left(\left|\frac{\partial f}{\partial u}\right|\right) \cdot h^k/N)$, $s_0 = -4.0 \cdot \log_{10} N$, $s_k = \log_{10} S_k$, $S_k = \min(C \cdot F_k, 1.0)$ and $C = 10^3 \cdot (5.0N^4)$. The variable κ is empirically chosen to obtain a sharp but smooth shock profile. In this work $\kappa = 2.0$.

The most notable characteristic of this approach is the ability to control Gibbs phenomenon even if the shock formation occurs inside a mesh element.

3.7 Time marching

The DG-FEM spatial discretization of the traffic flow equation produces a system of first order ODEs in terms of the traffic density field of the problem.

Before integrating the semi-discrete problem given by the Eq. (25) in time, we define the right hand side operator $\mathcal{L}_h$ for the variable $\boldsymbol{u}_h$ as

$$\mathcal{L}_h(\boldsymbol{u}_h,t)=\frac{2}{h^k}\mathcal{M}^{-1}\left\{\mathcal{S}^T\hat{\boldsymbol{f}}_h^k+\left[-\frac{1}{2}\,\mathcal{F}_l^{k+1}\left(\hat{\boldsymbol{f}}_h^{k+1}-C\hat{\boldsymbol{u}}_h^{k+1}\right)-\frac{1}{2}\mathcal{F}_r^k\left(\hat{\boldsymbol{f}}_h^k+C\hat{\boldsymbol{u}}_h^k\right)\right.\right.$$
$$\left.\left.+\frac{1}{2}\,\mathcal{F}_r^{k-1}\left(\hat{\boldsymbol{f}}_h^{k-1}+C\hat{\boldsymbol{u}}_h^{k-1}\right)+\,\frac{1}{2}\mathcal{F}_l^k\left(\hat{\boldsymbol{f}}_h^k-C\hat{\boldsymbol{u}}_h^k\right)\right]\right\} \tag{44}$$

or in the following alternative form when considering the add of the artificial viscosity operator

$$\mathcal{L}_h(\boldsymbol{u}_h,t)=\frac{2}{h^k}\mathcal{M}^{-1}\left\{\mathcal{S}^T\hat{\boldsymbol{f}}_h^k-(\mathcal{S}^{\sqrt{\varepsilon}})^T\hat{\boldsymbol{q}}_h^k+\left[-\frac{1}{2}\mathcal{F}_l^{k+1}\left(\hat{\boldsymbol{f}}_h^{k+1}-C\hat{\boldsymbol{u}}_h^{k+1}\right)-\frac{1}{2}\mathcal{F}_r^k\left(\hat{\boldsymbol{f}}_h^k+C\hat{\boldsymbol{u}}_h^k\right)\right.\right.$$
$$+\frac{1}{2}\mathcal{F}_r^{k-1}\left(\hat{\boldsymbol{f}}_h^{k-1}+C\hat{\boldsymbol{u}}_h^{k-1}\right)+\frac{1}{2}\mathcal{F}_l^k\left(\hat{\boldsymbol{f}}_h^k-C\hat{\boldsymbol{u}}_h^k\right)$$
$$\left.\left.+\sqrt{\varepsilon(x_r^k)}\,\mathcal{F}_r^k\hat{\boldsymbol{q}}_h^k-\,\sqrt{\varepsilon(x_r^{k-1})}\,\mathcal{F}_r^{k-1}\hat{\boldsymbol{q}}_h^{k-1}\right]\right\}, \tag{45}$$

$$\hat{\boldsymbol{q}}_h^k=\frac{2}{h^k}\mathcal{M}^{-1}\left\{-(\tilde{\mathcal{S}}^{\sqrt{\varepsilon}})^T\hat{\boldsymbol{u}}_h^k+\frac{1}{2}\left(\sqrt{\varepsilon(x_l^{k+1})}+\sqrt{\varepsilon(x_r^k)}\right)\mathcal{F}_l^{k+1}\hat{\boldsymbol{u}}_h^{k+1}\right.$$
$$\left.-\frac{1}{2}\left(\sqrt{\varepsilon(x_r^{k-1})}+\sqrt{\varepsilon(x_l^k)}\right)\mathcal{F}_l^k\hat{\boldsymbol{u}}_h^k\right\}. \tag{46}$$

To march this system of equations in time, we used the classical and reliable forth order four stage explicit Runge-Kutta method (ERK)

$$\begin{aligned}
\boldsymbol{k}^{(1)}&=\mathcal{L}_h(\boldsymbol{u}_h^n,t^n),\\
\boldsymbol{k}^{(2)}&=\mathcal{L}_h\left(\boldsymbol{u}_h^n+\frac{1}{2}\Delta t\boldsymbol{k}^{(1)},t^n+\frac{1}{2}\Delta t\right),\\
\boldsymbol{k}^{(3)}&=\mathcal{L}_h\left(\boldsymbol{u}_h^n+\frac{1}{2}\Delta t\boldsymbol{k}^{(2)},t^n+\frac{1}{2}\Delta t\right),\\
\boldsymbol{k}^{(4)}&=\mathcal{L}_h\left(\boldsymbol{u}_h^n+\Delta t\boldsymbol{k}^{(3)},t^n+\Delta t\right),\\
\boldsymbol{u}_h^{n+1}&=\boldsymbol{u}_h^n+\frac{1}{6}\Delta t\left(\boldsymbol{k}^{(1)}+2\boldsymbol{k}^{(2)}+2\boldsymbol{k}^{(3)}+\boldsymbol{k}^{(4)}\right),
\end{aligned} \tag{47}$$

to advance from $\boldsymbol{u}_h^n$ to $\boldsymbol{u}_h^{n+1}$ which are separated by the timestep, Δt. It is important to note that the ERK method is conditionally stable and requires the timestep size Δt be estimated using the CFL (Courant-Friedrichs-Lewy) condition. We define the CFL as

$$CFL:=\max_k\frac{c^k\Delta t}{\Delta x^k},$$

where c^k is the local propagation wave speed on element k and $\Delta x^k=h^k$ is the local spatial grid resolution. The specific value of the CFL (constant) number depends on the method used for the space and time discretizations but, in general, its order of magnitude is about 1. For high order methods such as the DG scheme described in this text, we have to consider the minimum grid space as the minimum distance between the mapped quadrature points (GL or GLL) on the mesh elements.

When considering the traffic flow equation with the artificial viscosity operator, the scaling of the explicit time step is tipically given by (Klockner et al., 2011)

$$\Delta t \sim \frac{1}{|V_{max}|\,\frac{N^2}{h} + \|\varepsilon\|_{L^\infty}\frac{N^4}{h^2}} \tag{48}$$

where V_{max} is the largest characteristic car speed, ε is the magnitude of the viscosity, h is the minimum local mesh size and N is the polynomial order of approximation.

4 NUMERICAL EXPERIMENTS

The traffic flow equation was solved for three different initial conditions: (1) Red light condition at the exit of the road; (2) Green light condition at half way of the road length and (3) Smooth exponential density configuration at the entrance of the road. All examples were set with appropriate Dirichlet or Neumann boundary conditions. For each initial condition described above: red light, green light and smooth configuration, the solutions were marched in time for 1.3, 2.0 and 1.2 minutes, respectively. The proposed DG-FEM scheme was compared to three different discretization schemes: (a) the 2^{nd} order MacCormack finite difference scheme (FDM); (b) the standard 1^{st} order finite volume scheme (FVM) and (c) the 2^{nd} order MUSCL finite volume scheme (MUSCL). Numerical solutions were compared based on the same number of degrees of freedom for each scheme, i.e., 220 nodes for FDM, 220 cells for FVM and MUSCL and 20 elements with polynomial order $N = 10$ for DG-FEM. 3D graphical representations of the numerical solutions along with 2D snapshots of important features revealed by each numerical scheme are showed in the next examples.

4.1 Red light

The red light example is a standard benchmark problem for the traffic flow equation as it has an exact solution described by a moving shock wave which travels backward from the exit to the entrance of the road. We examine a road of lenght $4\ Km$ where the speed limit is $V_{max} = 1.0\ Km/min$, fitting at most 10 cars per unit length ($u_{max} = 10.0\ cars/Km$). A red traffic light is located at the end of the road, $x = 4\ Km$. Cars accumulate quickly in the road exit, where we have the maximum allowed density of cars between $x = 3\ Km$ and $x = 4\ Km$, and there is an incoming traffic of 50% the maximum allowed density ($u = 0.5u_{max}$). This initial car density profile can be seen in Fig. (2).

Figure (3) shows a snapshot of the red light problem solution at the time $t = 1.2\ min$ considering all discretization schemes at once. This figure reveals some important details of each numerical solution. The 2^{nd} order FDM solution clearly showed an unphysical peak at the wave front demonstrating the absence of any control mechanism to deal with spurious oscillations around the discontinuity. Both 1^{st} order FVM and 2^{nd} order MUSCL schemes were able to sharply represent the discontinuous solution described by the square wave nevertheless with a saw-toothed shape due to their low order approximation properties (Van Leer, 1979). DG-FEM scheme with sub-cell shock capturing sharply represented the discontinuous solution with a smooth profile due to its high order numerical approximation properties.

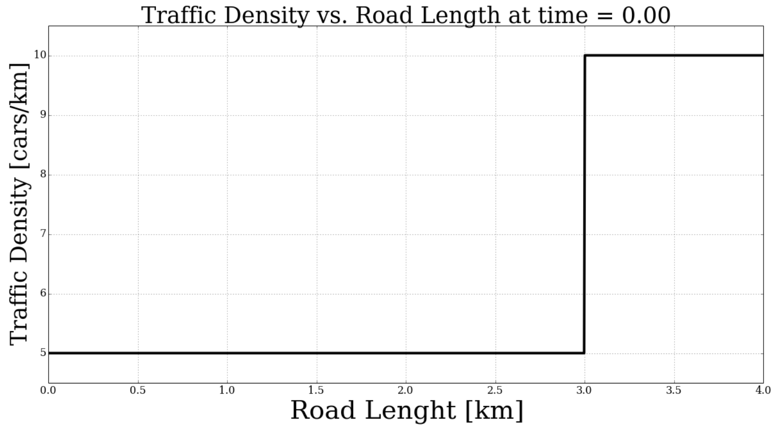

Figure 2: Red light initial condition

Figure 3: Red light example, all solutions at time $1.20\ min$

Figure (4) shows the 3D graphical representation of the numerical solutions of the red light problem for the four discretization schemes.

4.2 Green light

The green light example is an interesting case study for the traffic flow equation as it starts with a discontinuous profile at the wave front and develops a shock discontinuity at the rear of the propagating wave. As in the previous case, we consider the following setup parameters: road length, $4\ Km$, speed limit, $V_{max} = 1.0\ Km/min$, and maximum car density, $u_{max} = 10.0\ cars/Km$. We suppose there is a stoplight at the half way of the road where traffic is bumper-to-bumper, and the traffic density decreases linearly to zero as we approach the entrance of the road. Ahead of the stoplight the road is clear. This initial density profile is shown in Fig. (5).

Figure (6) shows a snapshot of the green light problem solution at the time $t = 1.05\ min$ considering all discretization schemes at once. This figure also reveals some remarkable details of each numerical solution. The 2^{nd} order FDM solution showed strong oscillations at the rear part of the wave evidencing the Gibbs' phenomenon around the shock formation. Both 1^{st} order

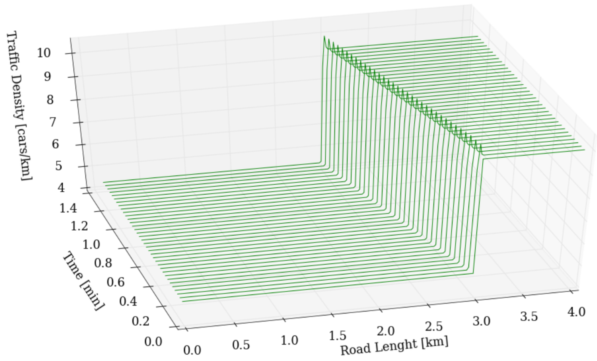

(a) FDM

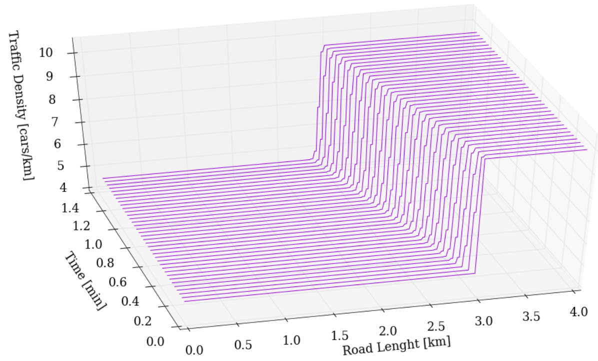

(b) FVM

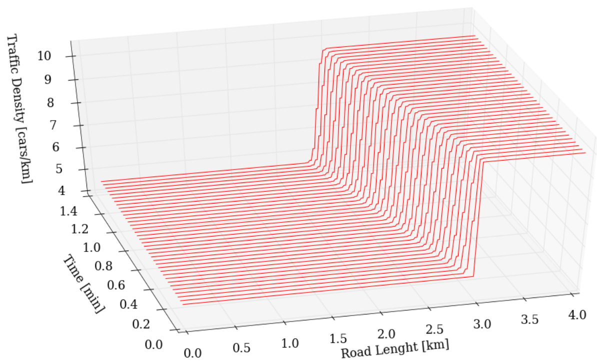

(c) MUSCL

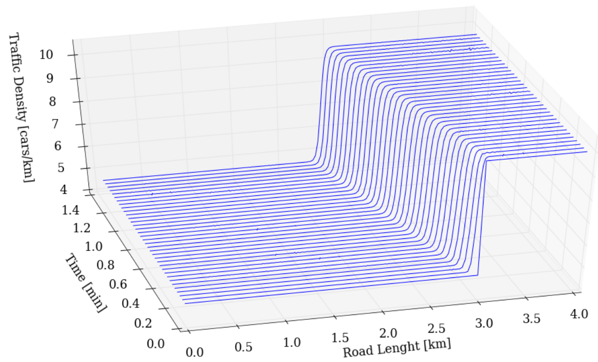

(d) DG-FEM

Figure 4: Red light problem solutions for the four discretization schemes

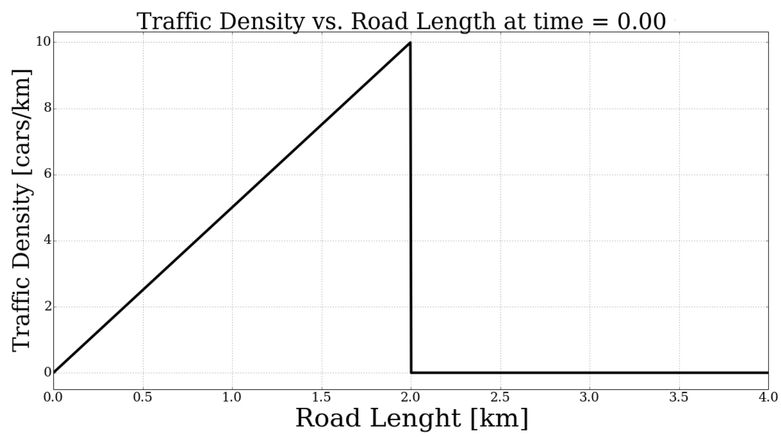

Figure 5: Green light initial condition

FVM and 2^{nd} order MUSCL schemes were able to sharply represent the discontinuous solution developed at the rear part of the wave as expected. However, they showed again a saw-toothed shape at the wave front typical of low order approximation schemes. DG-FEM scheme with sub-cell shock capturing sharply represented the discontinuous solution with a slightly over smeared wave shape particularly at the very rear of the moving wave.

Figure (7) shows the 3D graphical representation of the numerical solutions of the green light problem for the four discretization schemes.

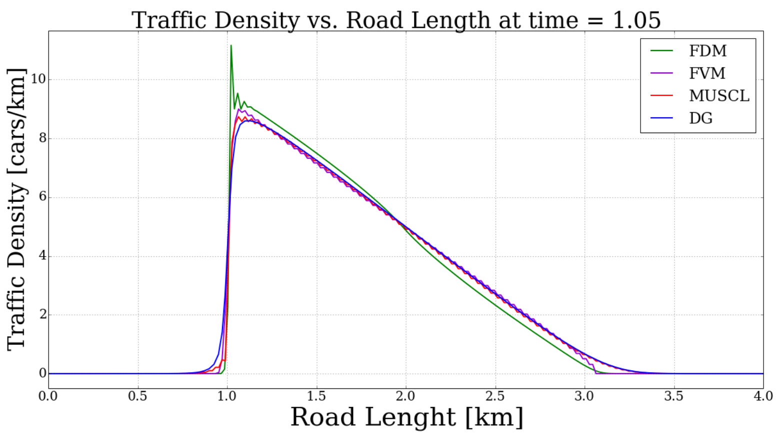

Figure 6: Green light example, all solutions at time $1.05\ min$

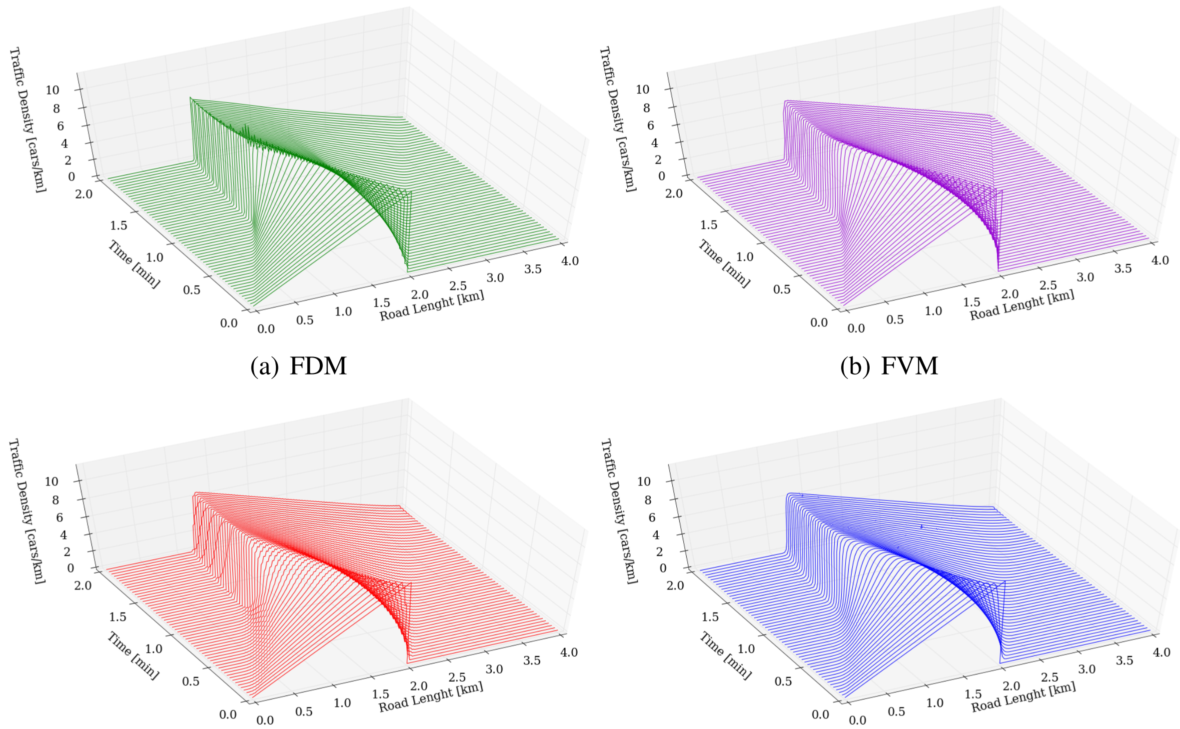

(a) FDM

(b) FVM

(c) MUSCL

(d) DG-FEM

Figure 7: Green light problem solutions for the four discretization schemes

4.3 Smooth initial condition

The exponential initial condition example is a rather theoretical case study for the traffic flow equation which shows a shock wave development from a very smooth initial profile. The setup parameters for this example were chosen as: road lenth, $2\pi\ Km$, speed limit, $V_{max} = 1.0\ Km/min$, and maximum traffic density, $u_{max} = 1.0\ car/Km$. The exponential initial condition is represented in Fig. (8).

Figure (9) shows a snapshot of the traffic flow problem solution with the exponential initial condition at the time $t = 1.05\ min$ considering all discretization schemes at once. This figure

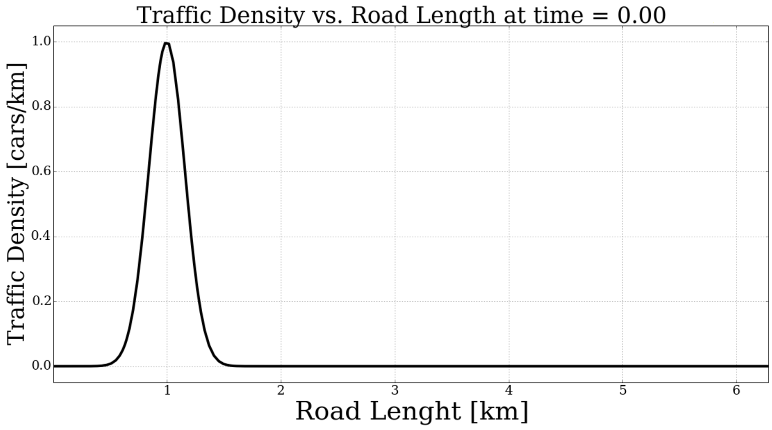

Figure 8: Exponential initial condition

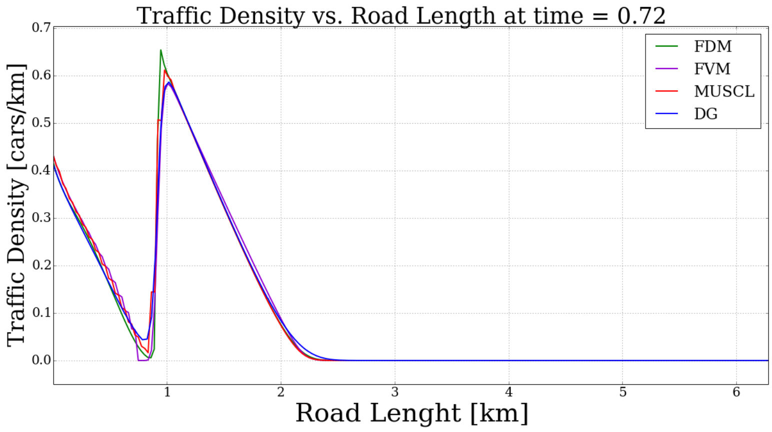

Figure 9: Smooth initial condition example, all solutions at time $0.72\ min$

shows common features between the present example and the previous ones. All numerical schemes were able to sharply capture the shock discontinuity upstream of the moving wave. The FVM and MUSCL schemes showed poor interpolating properties upstream of the shock formation. The FDM solution developed a sharp peak at the discontinuity region as expected due to the lack of a shock capturing stabilization mechanism in the MacCormack algorithm. DG-FEM scheme with sub-cell shock capturing showed a very good representation of the smooth wave profile with a slightly over smearing upstream the shock region.

Figure (10) shows the 3D graphical representation of the numerical solutions of the traffic flow problem with a smooth initial condition for the four discretization schemes.

5 CONCLUSIONS AND FUTURE WORK

This paper discussed the implementation of the high order discontinuous Galerkin (DG-FEM) technique to numerically solve the traffic flow equation based on the LWR model. Due to shock discontinuity formation in the solution of the many examples considered, a sub-cell shock capturing mechanism based on the introduction of small quantities of artificial dissipation along the time marching process was adopted. The proposed numerical scheme was compared

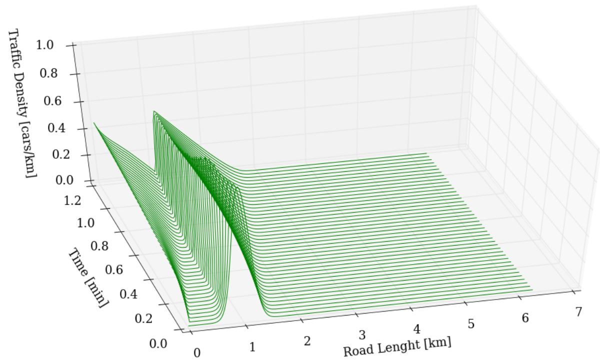

(a) FDM

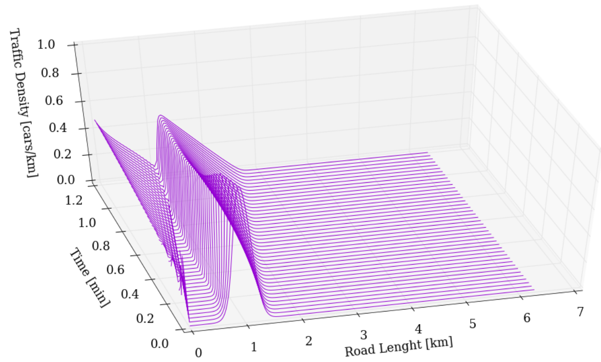

(b) FVM

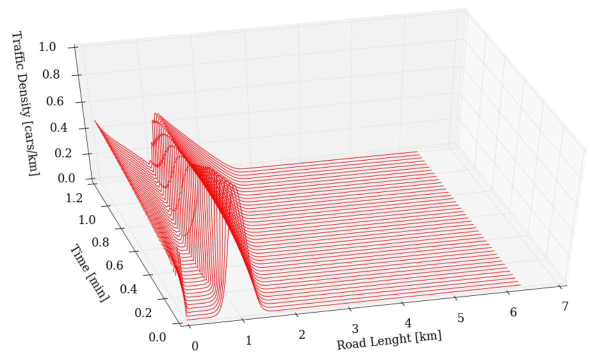

(c) MUSCL

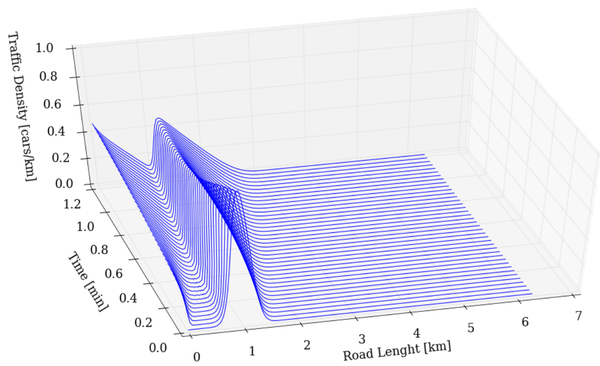

(d) DG-FEM

Figure 10: Smooth initial condition problem solutions for the four discretization schemes

to standard discretization algorithms such as the 2^{nd} order MacCormack FDM, a 1^{st} order FV algorithm and the 2^{nd} order MUSCL FV scheme with slope limiting mechanism. Comparisons were based on discretizations with the same number of degrees of freedom for each numerical scheme. Overall, the different schemes were capable to sharply represent the discontinuity in the solutions although the FDM approximation could not control Gibbs' phenomenon in the vicinity of shocks. The proposed DG-FEM solution with sub-cell shock capturing device showed promising results by sharply representing the shock wave profiles as well as the smooth regions of the solutions with remarkable accuracy. This numerical scheme also demonstrated great flexibility in dealing with mesh and polynomial order adaption. For future works we intend to extend this formulation for road networks and apply different techniques to control oscillations around shocks such as filtering and generalized slope limiters. We also expect to evaluate different time integrators such as strong TVD algorithms and implicit schemes.

ACKNOWLEDGEMENTS

The authors would like to thank the IBM Research Brazil laboratory for the technical support and funding. They also extend their gratitude to Paul Jean Louis Borrel from the same lab who offered great encouragement along the process of making relevant and impactful research.

REFERENCES

Barter, G. E. & Darmofal, D. L., 2010. Shock capturing with PDE-based artificial viscosity for DGFEM: Part I. Formulation, *Journal of Computational Physics*, vol. 229, n. 5, pp. 1810–1827.

Ceulemans, W., Wahab, M. A., De Proft, K. & Wets, G., 2009. Modelling Traffic Flow with Constant Speed using the Galerkin Finite Element Method, *Proceedings of the World Congress on Engineering*, vols I and II, pp. 993-999.

Greenshields, B. D., 1935. A study of highway capacity. *Highway Research Board Proceedings*, vol. 14, pp. 448-477.

Hesthaven, J. S. & Warburton, T., 2008. *Nodal Discontinuous Galerkin Methods: Algorithms, Analysis, and Applications*. Springer-Verlag.

Hirsch, C., 1990. *Numerical Computation of Internal and External Flows, Volume 2: Computational Methods for Inviscid and Viscous Flows*, John Wiley & Sons.

Karniadakis, G. E. & Sherwin, S. J., 2005. *Spectral/hp Element Methods for Computational Fluid Dynamics*, 2nd. ed., Oxford University Press.

Klöckner, A., Warburton, T. & Hesthaven, J. S., 2011. Viscous Shock Capturing in a Time-Explicit Discontinuous Galerkin Method, *Mathematical Modelling of Natural Phenomena*, vol. 6, n. 3, pp. 57-83.

LeVeque, R. J., 1990. *Numerical Methods for Conservation Laws*, ETH Lectures in Mathematics Series, Birkhauser-Verlag.

LeVeque, R. J., 2007. *Finite Difference Methods for Ordinary and Partial Differential Equations*, SIAM.

Lighthill, M. J. & Whitham, G. B., 1955. On kinematic waves II. A theory of traffic flow on long crowded roads, *Proceedings of the Royal Society of London, Series A, Mathematical and Physical Sciences*, vol. 229, n. 1178, 317–345.

MacCormack, R. W., 1969. The Effect of viscosity in hypervelocity impact cratering, AIAA Paper 69-354, *AIAA Hypervelocity Impact Conference, Cincinnati, Ohio, Apr. 30-May 02*.

Persson, P-O. & Peraire, J., 2006. Sub-Cell Shock Capturing for Discontinuous Galerkin Methods, *Proceedings of the 44th AIAA Aerospace Sciences Meeting and Exhibit*, volume 112.

Richards, P. I., 1956. Shock waves on the highway, *Operations Research*, vol. 4, n. 1, 42–51.

Suncica, C., Piccoli, B., Qiu, J. M. & Ren, T., 2015. Runge-Kutta Discontinuous Galerkin Method for Traffic Flow Model on Networks, *Journal of Scientific Computing*, vol. 63, n.1, pp. 233-255.

Van Leer, B., 1979. Towards the Ultimate Conservative Difference Scheme. V. A Second Order Sequel to Godunov's Method, vol. 32, pp. 101–136.